
SELF-PROPELLING COLLOIDAL FINITE STATE MACHINES

Steven van Kesteren^a, Laura Alvarez^{a,b}, Silvia Arrese-Igor^c, Angel Alegria^c, Lucio Isa^a

a. Laboratory for Soft Materials and Interfaces, Department of Materials, ETH Zurich, Zurich, Switzerland
b. CNRS, Univ. Bordeaux, CRPP, UMR5031, 33600 Pessac, France,
c. Centro de Física de Materiales (SCIC-UPV/EHU), Materials Physics Center, 20018 San Sebastián, Spain
lucio.isa@mat.ethz.ch

ABSTRACT

Endowing materials with physical intelligence holds the key for a progress leap in robotic systems. In spite of the growing success for macroscopic devices, transferring these concepts to the microscale presents several challenges connected to the lack of suitable fabrication and design techniques, and of internal response schemes that connect the materials' properties to the function of an autonomous unit. Here, we realize self-propelling colloidal clusters which behave as simple finite state machines, i.e. systems built to possess a finite number of internal states connected by reversible transitions and associated to distinct functions. We produce these units via capillary assembly combining hard polystyrene colloids with two different types of thermo-responsive microgels. The clusters, actuated by spatially uniform AC electric fields, adapt their shape and dielectric properties, and consequently their propulsion, via reversible temperature-induced transitions controlled by light. The different transition temperatures for the two microgels enable three distinct dynamical states corresponding to three illumination intensity levels. The sequential reconfiguration of the microgels affects the velocity and shape of the active trajectories according to a pathway defined by tailoring the clusters' geometry during assembly. The demonstration of these simple systems indicates an exciting route to build more complex units with broader reconfiguration schemes and multiple responses towards the realization of autonomous systems with physical intelligence at the colloidal scale.

Keywords Active matter, Colloidal molecules, Microrobots

1 Introduction

As automation increasingly pervades our lives, new paradigms for autonomous systems across a broad range of length scales and application fields are in high demand. The recent upsurge of soft robotics is a clear example, where strong efforts are currently underway to endow robots with physical intelligence [1]. This concept aims at transferring functions such as perception, control and response from computational units to physical agents toward the realization of robotic materials, i.e. materials that can perform one or more of these functions without external logic and that can be integrated in autonomous devices [2]. A simple guidance to constructing these systems can be based on the concept of a finite state machine (FSM). This model describes the behavior of a system as being defined by a finite number of different internal states connected by reversible transitions triggered in response to a defined set of inputs. An FSM description perfectly befits the scope of a robotic material, in the sense of a material whose function depends on its state, e.g. solid/liquid, expanded/contracted, soft/stiff, conductive/non-conductive, etc., and which can be switched by a specific trigger, e.g. temperature, light or electromagnetic signals.

Even if the implementation of these concepts is rapidly becoming more frequent at the macroscopic scale [3, 4, 5], its extension to the (sub)-micrometric or colloidal scale still presents significant challenges. Current microscale systems focus on self-propelling particles, aka artificial microswimmers or active colloids. These systems comprise units that can spontaneously convert an energy input, either externally supplied, e.g. in the form of an electromagnetic or acoustic field, or internally accessible, such as chemical fuel, into directed motion or self-propulsion. This kind of motility is at the core of the current and future applications of microswimmers to act as delivery vehicles [6, 7, 8, 9], active mixers [10], or remediation agents [11, 12], to name a few. Crucially, self-propulsion is enabled by the fact that active

colloids have an intrinsic asymmetry in their geometrical or compositional properties, which defines the directionality of their motion [13, 5]. However, this asymmetry is typically fixed during synthesis and fabrication[14], implying that synthetic microswimmers only have one internal state, and that propulsion is regulated by controlling the energy input.

The application of an FSM model to an active colloidal material requires the following features: i) a self-propulsion mechanism that depends on the particle’s state, i.e. shape or internal properties; ii) the possibility to reversibly switch between different states in response to well-defined inputs; iii) the possibility to encode the states and their transitions in a deterministic fashion during fabrication.

In this work, we fulfill these requirements by fabricating artificial microswimmers constituted by colloidal clusters or “molecules”[15, 16, 17], which combine responsive and non-responsive particles[18]. The clusters are deterministically prepared by means of sequential capillarity-assisted particle assembly (or sCAPA)[19]. They furthermore exhibit self-propulsion under spatially uniform AC electric fields in the kHz region, which are applied perpendicularly to the electrodes over which the particles move thanks to asymmetric electrohydrodynamic flows (EHDFs) [20, 21, 22, 23]. The transition between the different dynamical states is triggered by externally-imposed temperature signals, which cause the reconfiguration of the shape and dielectric properties of the clusters. We first begin by conceptually describing our approach to achieve microswimmers with multi-state dynamics and then focus on their experimental realization and characterization.

1.1 Self-propelling colloidal finite state machines: the concept

The conceptually simplest case of a self-propelling particle with multiple dynamical states is a two-state particle. Given the requirement for asymmetry, a two-state active particle can be realized by constructing a dumbbell where one of the two lobes changes its properties in response to an input signal.

By selecting EHDF-induced propulsion and temperature signals, dumbbells comprising one non-responsive, e.g. polystyrene (PS), lobe and one responsive, e.g. Poly(N-isopropylacrylamide)-based, lobe fulfill the criteria. Poly(N-isopropylacrylamide) (PNIPAM) is a thermo-responsive polymer that undergoes a reversible lower critical solubility transition at a well-defined temperature. PNIPAM-based particles (or microgels) correspondingly undergo a swelling/deswelling transition at that temperature, called the volume phase transition temperature or VPTT. Upon crossing the VPTT, microgels experience a volumetric change coupled to a variation of their dielectric properties [24, 25, 18, 26]. Self-propulsion generated by EHDFs in dumbbells depends both on the relative dimensions of the two lobes and on their dielectric properties [21, 13]. The existence of two different dynamical states for reconfigurable, PNIPAM-based active dumbbells has in fact been recently demonstrated [18].

However, the VPTT of the microgels depends on their chemistry, their internal architecture, e.g. crosslinking density [27], and the solvent properties [28]. In this work, we synthesize and use two types of thermo-responsive PNIPAM-based microgels to enable the access of multiple dynamical states (see Methods). In particular, we use two different comonomers, methacrylic acid (MAA) and acrylic acid (AA), in the polymerization of PNIPAM to obtain microgels with different VPTTs. The PNIPAM-co-MAA microgels have a green-fluorescent (BODIPY) core and the PNIPAM-co-AA microgels have a red-fluorescent (Nile-red) core, and are henceforth termed green (G) and red (R) microgels. Due to the higher hydrophilicity of AA compared to MAA, its VPTT is shifted to higher temperatures [29, 30, 31]. The VPTT of green-core microgels is $T_{G \rightleftharpoons G'} \approx 29$ °C and the one of the red-core microgels is $T_{R \rightleftharpoons R'} \approx 33$ °C (see Supplementary Section 1 for further details).

By using these microgels, we can therefore construct two different types of dumbbells, G-PS and R-PS, respectively, of which we can schematically represent the different states and their transitions as shown in Figure 1A. The G-PS dumbbells undergo a transition between a swollen state G to a collapsed state G' ($G \rightleftharpoons G'$) at a temperature $T_{G \rightleftharpoons G'}$, and correspondingly the transition $R \rightleftharpoons R'$ takes place at $T_{R \rightleftharpoons R'}$. As it will be showed in Section 1.2, these two transitions correspond to a switch between two different self-propulsion modes, with an adaptation of the propulsion velocity $V_G \rightleftharpoons V_{G'}$ and $V_R \rightleftharpoons V_{R'}$, respectively.

The existence of two different transition temperatures opens the way to the fabrication of microswimmers with three distinct dynamical states by incorporating both G and R microgels in a colloidal trimer together with a PS particle, as schematically shown in Figure 1B. Upon crossing $T_{G \rightleftharpoons G'}$, the trimer goes from a fully swollen state to one where only the G microgel is collapsed $GR \rightleftharpoons G'R$; when $T_{R \rightleftharpoons R'}$ is crossed, both microgels collapse and the trimer undergoes the $G'R \rightleftharpoons G'R'$ transition. The order of the transitions is reversed by progressively reducing temperature. In the case of the trimer, because the collapse of one microgel can cause the breaking of the axial symmetry of the cluster, in addition to three distinct translational velocities $V_{GR} \rightleftharpoons V_{G'R} \rightleftharpoons V_{G'R'}$, three different angular velocities can also be accessed $\omega_{GR} \rightleftharpoons \omega_{G'R} \rightleftharpoons \omega_{G'R'}$.

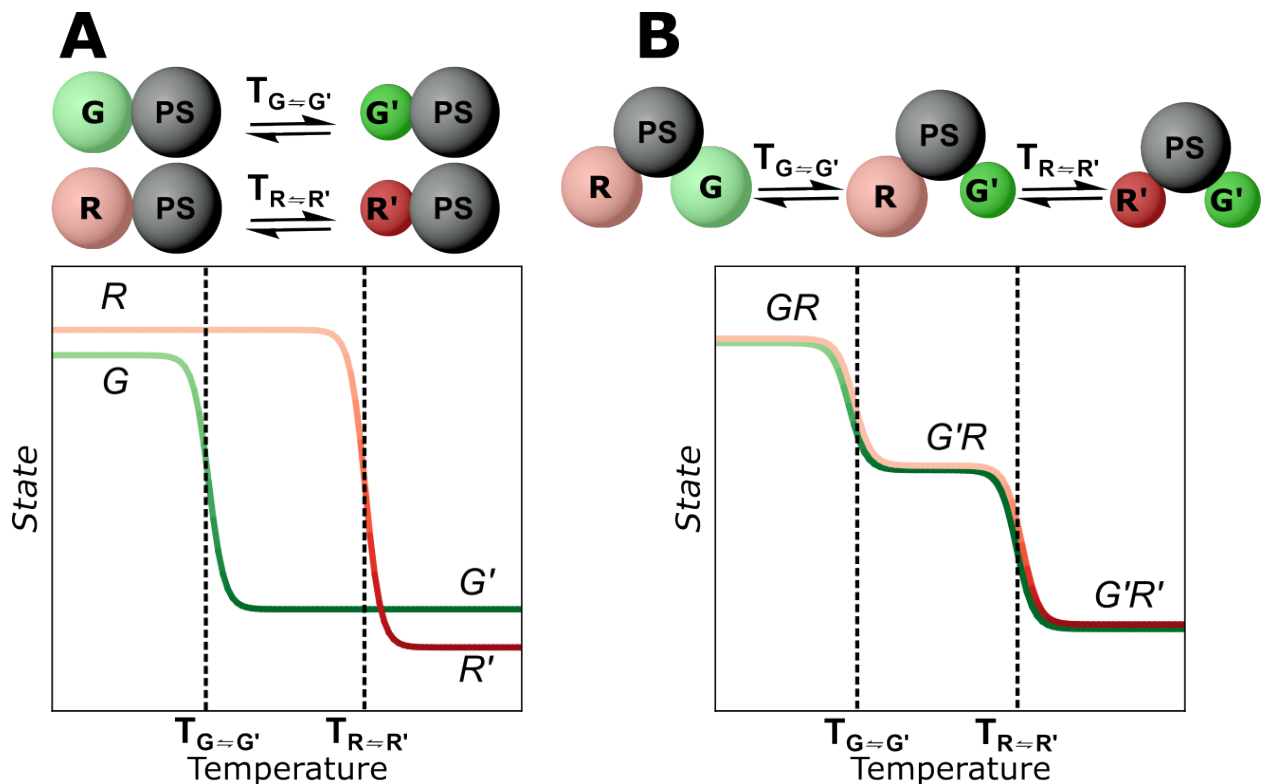


Figure 1: **Schematic representation of the FSM model for reconfigurable colloidal clusters.** A, Representation of the reconfiguration of the of G-PS and R-PS dumbbells upon crossing the respective transition temperatures $T_{G=G'}$ and $T_{R=R'}$ and schematic of the corresponding transition between the different states as a function of temperature T . B, Extension of the previous concept to a three-state particle (R-G-PS trimer).

1.2 Two-state dynamics: self-propelling responsive dumbbells

After introducing the concept in the previous Section, we now show that the behavior schematically displayed in Figure 1A can be experimentally implemented. We synthesized PNIPAM-co-MAA (G) microgels and PNIPAM-co-AA (R) microgels that have a hydrodynamic diameter of $\approx 2\text{-}3\ \mu\text{m}$ before and $\approx 0.7\text{-}1.2\ \mu\text{m}$ after their respective VPPT (Figure S4). In both cases the fluorescent cores are made from poly 2-trifluoromethylacrylic (PTFMA) and have a diameter of around 200 nm, to visualize the different microgels under the microscope. The G-PS and R-PS dumbbells are obtained using sCAPA, as previously described [19, 18]. In short, both PS particles and microgels are sequentially deposited into pre-designed traps microfabricated on a polydimethylsiloxane (PDMS) template. An evaporating droplet of the target particle suspension is moved over the PDMS template at a controlled speed and capillary forces selectively place the particles inside the traps. PS particles are deposited first, followed by either the G or R microgels to obtain the dumbbells inside the traps (see Figure 2A-B). After deposition, the particles are linked by thermal sintering at 75°C for 15 minutes and harvested using an adhesive sacrificial layer of glucose.

The resulting dumbbells are dispersed in a dilute HEPES buffer and confined between two transparent electrodes consisting of glass slides coated by a Cr and a Au layer covered with a polyethylene glycol (PEG) brush (see Methods). The electrodes are separated by a $240\ \mu\text{m}$ spacer and connected to a function generator that applies an AC electric field of 7 V peak-peak amplitude ($300\ \text{V cm}^{-1}$) and 800 Hz frequency perpendicular to the electrodes. Upon application of the AC field, both the electrodes and the particles polarize; the presence of the particles close to the bottom electrode (where they sediment) causes a local distortion of the electric field generating a component that is tangential to the substrate, which in turns leads to the recirculation of ions, the so-called electrohydrodynamic flows (EHDFs), around each colloid [20]. At a fixed voltage and frequency, the magnitude of the EHDFs depends on the particle size and dielectric properties [13, 21, 20]. However, for homogeneous spherical particles, the EHDFs are radially symmetric and do not induce any net propulsion. Conversely, for dumbbells with lobes of different size and dielectric properties, the symmetry of the EHDFs is broken and a net fluid flow is generated, which leads to self-propulsion. In particular, if U_i is the magnitude of the velocity of the EHDF generated around particle i , the propulsion velocity of the dumbbell can be

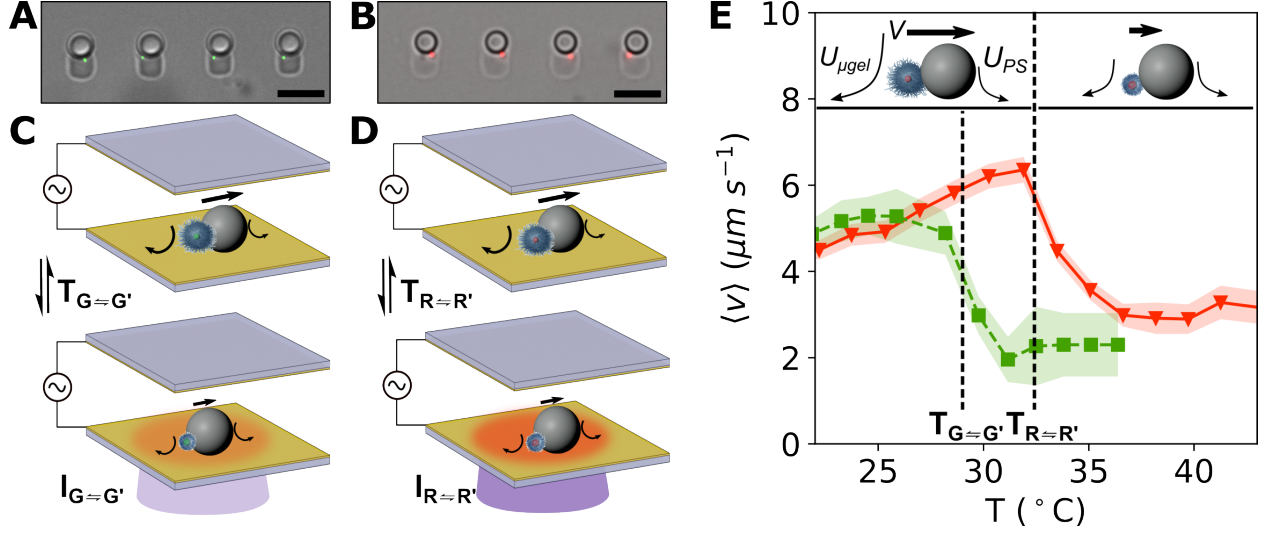


Figure 2: **Two-state microswimmers.** A-B, Combined bright-field+fluorescence micrographs of G-PS (A) and R-PS (B) dumbbells in the sCAPA traps. The scale bars are 5 μm . C-D, Schematic of the experiment for the two-state temperature-induced switching in the self-propulsion of G-PS (C) and R-PS (D) dumbbells. The curved arrows indicate the EHDFs generated by the PS and microgel lobes, respectively, and the straight arrows represent the net propulsion due to these EHDFs. Plasmonic heating of the substrate illuminated with a light of intensity $I_{G=G'}$ ($I_{R=R'}$) raises the local temperature above $T_{G=G'}$ ($T_{R=R'}$) inducing a phase transition in the microgels. Note that because $T_{R=R'} > T_{G=G'}$, the corresponding illumination intensity is higher. E, Mean instantaneous self-propulsion velocity $\langle v \rangle$ as a function of temperature T for the R-PS (triangles) and G-PS (squares) dumbbells. The shaded bands are the 99% confidence intervals calculated over 350 and 70 particles for the R-PS and G-PS, respectively. The vertical dashed lines mark the transition temperatures for the green and red core microgels, respectively. The inset schematically shows the switching of the self-propulsion state upon crossing the critical temperature, taking a R-PS dumbbell as an example. The curved arrows represent the EHDFs generated by the microgel and the PS particle, with characteristic velocities $U_{\mu\text{gel}}$ and U_{PS} , respectively, and the straight arrows indicate the net propulsion with velocity V .

written, in first approximation, as $v_{ij} = U_i r_j + U_j r_i / (r_i + r_j)$, where r_i is the radius of particle i (or j , respectively) [21]. Given that both U_{PS} and r_{PS} do not strongly depend on temperature, a sudden change in propulsion velocity is expected upon crossing $T_{G=G'}$ and $T_{R=R'}$ for the G-PS and R-PS dumbbells, respectively, because both the size and the dielectric properties of the microgels switch between different states upon crossing their respective VPTT (see Supplementary Section 2 for further details).

Experimentally, we induce controlled and rapid temperature variations by exploiting the plasmonic heating of the Au layer within the electrode upon illumination at 395 nm and 555 nm [32]. By adjusting the light intensity, we can locally heat the system above $T_{G=G'}$ or $T_{R=R'}$ and correspondingly reconfigure the dumbbells (2A-B; (see Supplementary Section 3 for further details) for an experimental calibration and a numerical verification of the heating via finite element modelling (FEM) with COMSOL Multiphysics [33]). The system equilibrates within seconds and cools down upon removal of the illumination to ensure the reversible transition between the different states.

In line with previous observations [18], the collapse of the microgels significantly reduces the magnitude of the propulsion velocity of the microgel-polystyrene dumbbells (Figure 2C). In particular, $T_{G=G'}$ or $T_{R=R'}$ are sufficiently separated so that G microgels collapse while R ones are still in the swollen state, resulting in reconfiguration and velocity changes at distinct temperatures. This response follows the scheme proposed in 1A and holds the key to access additional dynamical states when combining both microgels in one active cluster.

1.3 Assembly of multi-microgel colloidal clusters

However, in order to realize the system proposed in Figure 1B, we need to achieve deterministic control on the relative position of the two microgels in the active G-R-PS trimer. As it can be seen in 2A-B, conventional sCAPA in rectangular traps does not have sufficient positional control for the microgels, which are deposited on either side of the PS particles. In order to overcome this limitation, we have recently demonstrated a further refinement of sCAPA that exploits

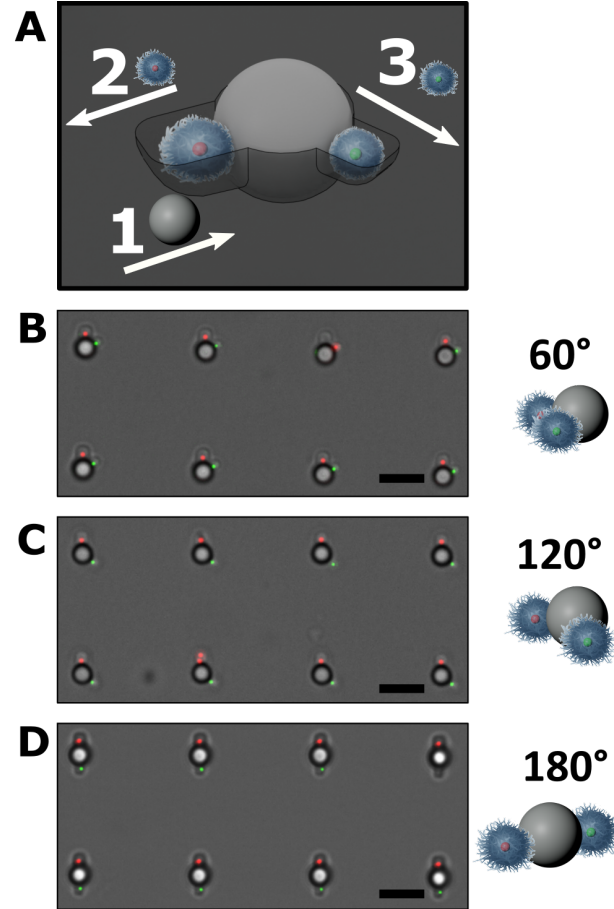


Figure 3: **Assembly of reconfigurable trimers.** A, Schematic showing the filling of the 3D-traps with sCAPA for a single colloidal 120-cluster. The numbers indicate the order of the deposition steps and the arrows respective deposition directions. B-D, Combined bright-field+fluorescence micrographs of R-G-PS trimers in the sCAPA traps with 60 (B), 120 (C) and 180 (D) degrees between the microgels. Scale bars are 5 μm

traps with three-dimensional height profiles realized by direct writing using a two-photon nanolithography system (Nanoscribe GT2 Professional), as schematically shown in Figure 3A-B (see Methods and Supplementary Section 4 for further details).[34] We use the different height of the different sections of the trap to guide the deposition of the polystyrene particles and the R and G microgels into trimers with well-defined opening angles. The assembly process requires careful tuning of the trap geometry as well as of the deposition medium, speed, direction and order [35]. In particular, the PS particles are deposited first, followed by the R and then the G microgels (see Figure 3B). By changing the geometry of the traps, we produced three-particle clusters with opening angles of 60, 120 and 180° degrees. We refer to these systems as 60-, 120-, or 180-clusters and examples are shown in Figure 3C. The deposition yields go up to 75% for the 120-clusters (see Supplementary Section 5 for further details) and we use the same linking and harvesting procedures as for the dumbbells.

1.4 Three-state motility of 120-clusters

We first focus on the dynamical response of the 120-clusters. After assembly and harvesting, the trimers are inserted in the same experimental cell that we previously described for the dumbbells and the transverse AC electric field (7 V peak-to-peak at 800Hz) is applied together with illumination of varying power density I at 395 nm to induce the local heating (Figure 4A). In particular, we use a sequence of illumination/heating steps in the following order: 30 s no illumination ($\approx 21^\circ\text{C}$), 60 s at 33 mW mm^{-2} ($\approx 31^\circ\text{C}$), 30 s at 92 mW mm^{-2} ($\approx 45^\circ\text{C}$) and finally 60 s no illumination (Figure 4B). This sequence enables us to switch between a state where both microgels are swollen (GR), one where one microgel is swollen and the other one is collapsed ($G'R$), one where both microgels are collapsed ($G'R'$) and back to the initial state where both microgels are swollen again (GR) (Figure 4B). We observe rapid, reversible switching

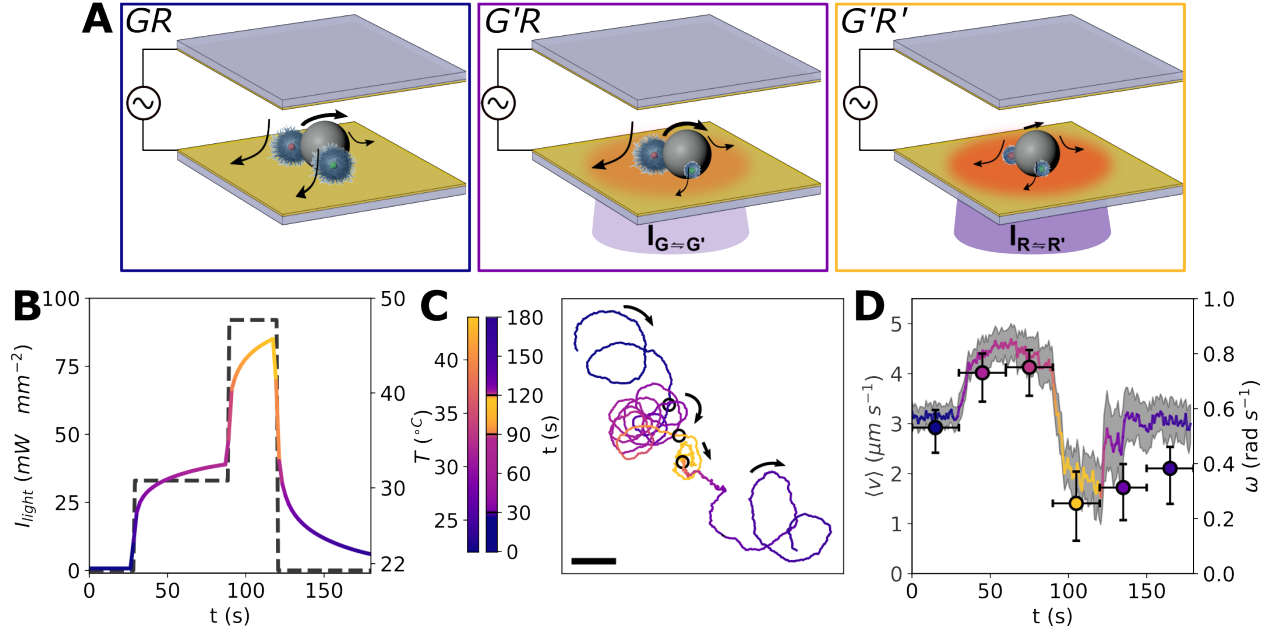


Figure 4: **Three-state dynamics for G-R-PS 120-clusters.** A, Schematic illustrating the 120-cluster in state (GR), ($G'R$), or ($G'R'$) depending on the illumination conditions. The arrows indicate the EHDFs and the net propulsion like in the previous figures. B, Light exposure sequence (dashed line) over time and resulting temperatures (solid line) as predicted by finite elements simulations. The color coding of the temperature corresponds to the color scale bar on the right of the graph. C, Example trajectory of a G-R-PS 120-cluster color-coded with time and corresponding temperature as represented by the color scale bars on the left of the graph. The scale bar is 20 μm . D, Mean instantaneous velocity (solid line) and angular velocity (symbols) of the microswimmer over time color-coded with temperature. The shaded bands and vertical error bars are the 99% confidence intervals calculated over 39 trajectories for the instantaneous velocity and angular velocity, respectively.

amongst the various states, which is reflected in a qualitative and quantitative variation of the trajectories (Figure 4C): in state (GR) the trajectory is curvilinear with a constant radius of $\approx 12\mu\text{m}$, in ($G'R$) the particle continues with a strong chiral motion but the radius of curvature is significantly decreased to $5.5\mu\text{m}$, and, finally, in ($G'R'$) the propulsion velocity drops and the rotational diffusion increases, resulting in less-directed motion. Upon removal of fluorescence illumination, the trajectory resumes the original shape of state (GR).

By quantitatively tracking the motion of the trimers as a function of time/illumination, we further characterize their motility in terms of their instantaneous and angular velocity. The two quantities are coupled due to the nature of the trajectory (Figure 4D), but they can be independently measured from the experiments (see Supplementary Section 6 for the calculation of the angular velocity) and both contribute to how the active particles explore space (see Figure 5). The shape of the trajectories and net swimming velocity are rationalized by considering the direction of the propulsive force and of viscous drag. As we have previously discussed in Figure 1, in the case of dumbbells, propulsion is aligned with the direction of compositional asymmetry and, as a consequence of geometry, the center of propulsion and of hydrodynamic drag coincide. However, this is not necessarily the case for the trimers. As schematically shown in Figure S12 (Supplementary Section 7), we can rationalize the propulsion of the trimer as the linear superposition of the propulsion generated by two dumbbells, respectively connecting the PS particles to the G and the R microgels. Variations in the magnitude of each velocity vector and of the size of the respective dumbbell lobes, may cause a misalignment between the center of propulsion and the center of hydrodynamic drag, giving rise to a rotation-translation coupling and the corresponding emergence of an active torque[36, 37, 38, 39]. With this simple image in mind, and considering the temperature response of each individual self-propelled dumbbell, in state (GR), each microgel has a similar size and generates similar EHDFs. However, these are not identical, leading to a breaking of the in-plane symmetry of the trimer's propulsion and drag, which leads to a curvilinear trajectory with a well-defined chirality and a large radius. In ($G'R$), the G-microgel collapses with a dramatic drop on its propulsion velocity, while the propulsion velocity of the R-microgel increases slightly. The greater asymmetry between both microgels leads to an increased torque, and correspondingly to a tightening of the curvilinear radius. The $G'R$ -trimer's instantaneous velocity is slightly larger compared to the one in state (GR), due to the moderate increase of the EHDFs of the R-PS dumbbell, in

conjunction with the reduced drag stemming from the collapse of the G-microgel. The combination of these factors leads to an increased angular velocity. Finally, in ($G'R'$), both microgels are collapsed and provide a significantly lower propulsive force. Correspondingly, the trimer's velocity dramatically drops. This fact, combined with the overall decreased size of the microswimmer implies that rotational diffusion plays a greater role in determining the trimer's trajectory in state ($G'R'$).

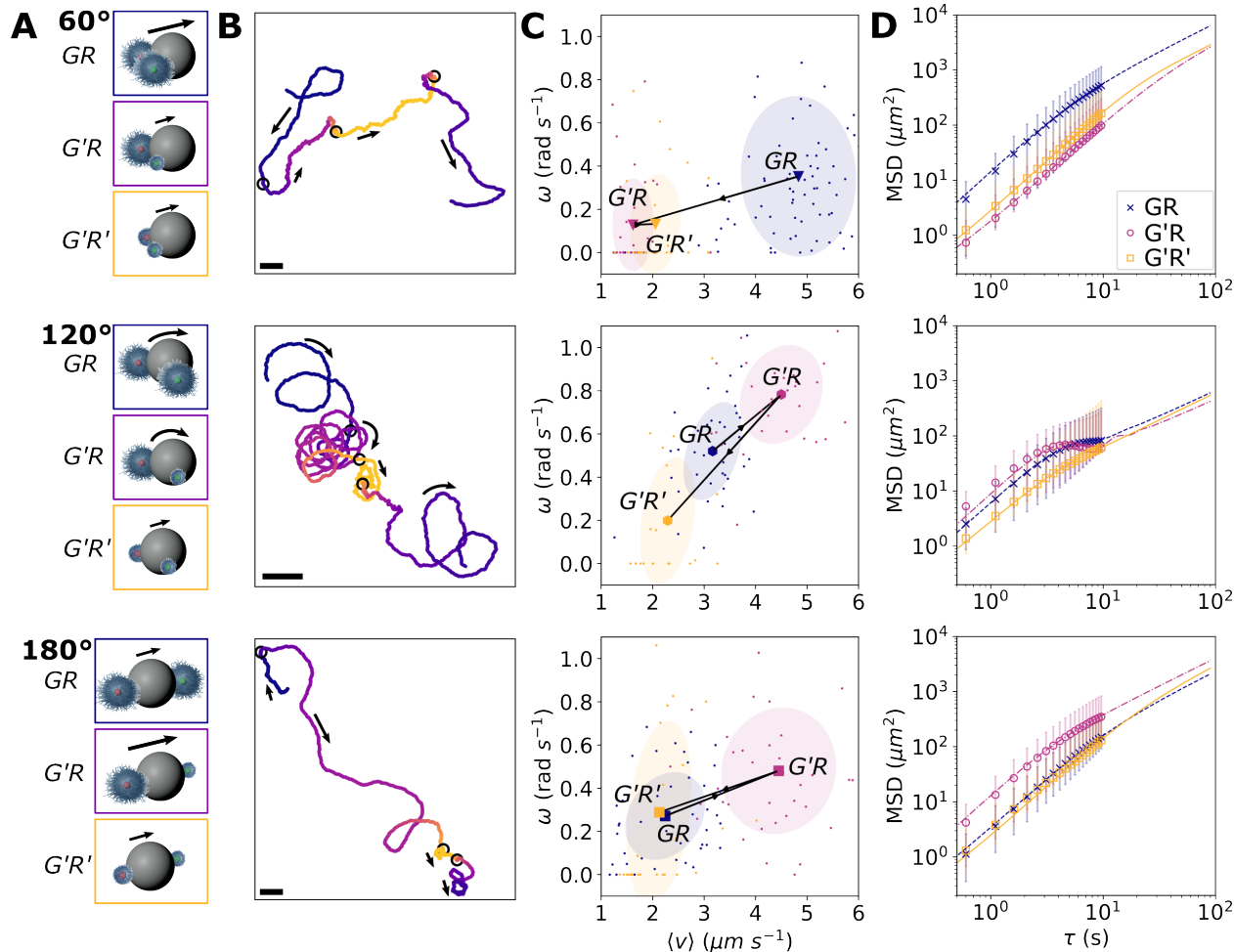


Figure 5: **Multi-state motility of different active clusters.** Each row corresponds to the 60-, 120- or 180-clusters, respectively. A, Schematic of the representative motion of the three clusters in state (GR), ($G'R$) and ($G'R'$). B, Example trajectories color-coded with temperature (same temperature range as in Figure 3). Scale bars are $20 \mu\text{m}$. C, Scatter plot of the mean instantaneous velocity and angular velocity for each particle in (GR), ($G'R$) and ($G'R'$). The elliptical shaded regions correspond to one standard deviation of both quantities calculated over 54, 39 and 45 trajectories for the 60-, 120- or 180-clusters, respectively. D, Ensemble-averaged MSD in (GR), ($G'R$) and ($G'R'$). Symbols: experimental data. Dashed lines: MSD fits for a rotating active Brownian particle [40].

1.5 Multi-state space exploration

The same simplified approach can be used to describe the motility of trimers with the other internal angles (see Supplementary Section 7 for further details), where reconfiguration can be used to tune how different active clusters explore space. By examining active trajectories, we immediately observe a clear qualitative difference in the dynamical behavior amongst the 60-, 120- and 180-clusters (Figure 5A).

The 60-clusters (Figure 5A top) have the largest instantaneous velocity in state (GR). However, unlike the 120-clusters, their velocity immediately drops in ($G'R$) and remains similar in ($G'R'$). The 180-clusters (Figure 5A bottom) conversely have a low instantaneous velocity in state (GR) compared to the 120-cluster. However, the transition to state ($G'R$)

shows a much more significant speeding up without a large change in the angular velocity, while in state ($G'R'$) the 180-cluster behave very similar to the 60- and 120-clusters. We therefore show that simple reconfiguration strongly affects the motility of the clusters in the different states.

Similarly to our description of the 120-cluster, the behaviour of the 180-cluster can be rationalized by the force vector model shown in the Supplementary Section 7. In state (GR) the propulsive forces of the 2 microgel-PS dumbbells are similar in magnitude but oppose each other leading to a very small net propulsion. Switching to ($G'R$) breaks this balance, the G microgel collapses and the clusters speed up. However, the behaviour of 60-clusters appear different, and self-propulsion essentially ceases already at $T_{G=G'}$ and does not change upon crossing $T_{R=R'}$. We hypothesize that, given their dimensions relative to the PS particle, the two microgels substantially overlap in the swollen state with an internal angle of 60° , such that the collapse of the G microgel already causes the R microgel to collapse, practically eliminating any difference between ($G'R$) and ($G'R'$) (see Supplementary Section 8 for further details).

Finally, the three different states of the clusters are associated with different ways to explore space, which can be represented by plotting their mean-square displacements (MSDs) [40]. The 60- and 180-cluster have a clear 'fast' state, which is (GR) for the 60-clusters and ($G'R$) for 180-clusters. These states correspond to high instantaneous velocities and small angular velocities explore, for which space is explored significantly faster by particle ensembles than the low-velocity states at any time. The MSDs for 120-cluster are more nuanced, where mean displacements are greater in state ($G'R$) at short times, but motion becomes more confined at longer times due to the strong chiral motion. The distinct dynamical behavior of different clusters in different states indicates a broad range of possibilities to develop adaptive artificial microswimmers by design.

2 Conclusions and outlook

In this manuscript we have demonstrated that the combination of deterministic assembly using sCAPA and the utilization of stimuli-responsive microgels enables the realization of synthetic microswimmers that can transition among distinct internal states, which are in turn coupled to their dynamics. Importantly, and differently from typical light- or magnetically-activated particles, where the stimuli for propulsion and the ones that regulate motility coincide [4, 41, 42], our system's propulsion mechanism is orthogonal to the reconfiguration one.

The current study focuses on demonstrating the feasibility of self-propelling finite state machines at the colloidal scale and on the characterization of the single-particle dynamics for different microswimmer designs. However, the independence of the reconfiguration pathway enables robust control of the particle motility and the possibility to easily implement spatially and temporally-modulated motility landscapes to investigate collective effects, in analogy with investigations of the collective dynamics of light-regulated bacteria [43, 44]. In living organisms, the adaptation to external stimuli is internally regulated and characterized by finite transition times. Conversely, synthetic microswimmers subjected to sophisticated perception and adaptation schemes [45, 46, 47] are externally controlled and the feedback between input signals and motility regulation can be considered instantaneous over the characteristic timescales of active motion. Nonetheless, the presence of finite response times, even for external control strategies, has been shown to lead to emergent dynamical and collective effects [48, 49, 50]. Our colloidal FSMs fall in between these categories, where propulsion and reconfiguration are externally triggered, but where the transitions between the different states are encoded during fabrication and take place with a characteristic internal time scale.

Given our findings, many further avenues for future work open up. For instance, the level of single-particle control may already be amenable to the demonstration of lab-on-chip devices. The AC-electrodes could be easily integrated in microfluidic systems, where, guided by thermal signals, the reconfigurable microswimmers can navigate and perform different functions. For example, we envisage that the 60-clusters accumulate in regions where the temperature is between 29-33 °C, corresponding to state ($G'R$), where they have a small MSD. They could therefore efficiently explore space in *state GR* until they reach a region with a higher temperature and linger there, i.e. to aid or perform a chemical reaction, if carrying the appropriate load. Conversely, in the same state, 180-clusters would spend little time in these hotter regions due to a corresponding increase in their MSDs. They could thus be used to remove reaction products and transfer them to colder regions, where their motility drops. Even though thermal signaling may not be practical for all applications, incorporating responses to different stimuli may offer further options.

In fact, the modular assembly enabled by sCAPA makes it possible to incorporate other soft components, which can reconfigure in response to different stimuli. PNIPAM-based microgels that are responsive to light [51], pH [30, 31], redox state [52], magnetic fields [53] and (bio)chemical molecules [54] have been synthesized. The use of multiple, orthogonal stimuli would greatly increase the number of possible states, compared to using only one stimulus, e.g. temperature, with different transitions.

Finally, in order to successfully assemble precisely-programmed reconfigurable clusters, we had to push the boundaries of sCAPA beyond the state of the art with the introduction of 3D height profiles within the traps to direct the deposition of soft and hard particles in deterministic shapes. In the future, we also envisage that additional strategies can be used to incorporate reconfigurable parts in microscale active units. Recent advances in 3D-printing of microscale responsive hydrogels with two-photon nanolithography could allow for more flexible fabrication of soft structures [55], toward hybrid colloidal materials[56]. All of these efforts will take a very active community of researchers and engineers one step, or more, closer to the goal of realizing autonomous microscale systems with capabilities mirroring the ones of larger scale robotic units.

Acknowledgements

LA acknowledges financial support from the European Soft Matter Infrastructure (EUSMI) proposal number S180600105. This project has received funding from the European Research Council (ERC) under the the European Union's Horizon 2020 research and innovation programme grant agreement No 101001514. We thank Alexander Kuehne and Dirk Rommels for help with particle synthesis and discussion.

3 Materials and Methods

All chemical if not state otherwise were used as provide by the supplier. Triton X-45, Acrylic acid (AA),Methacrylic Acid (MAA), N, N' Methylenebis(acrylamide) (BIS), 2,2,2-Trifluoroethyl methacrylate (TFMA), Sodium dodecyl sulfate (SDS), Potassium persulfate (KPS), BODIPY, and Nile red were purchased from Sigma-Aldrich. N-Isopropylacrylamide (NIPAM) was purchased from Sigma-Aldrich and purified by recrystallization in Toluene/Hexane 50:50. 4-(2-hydroxyethyl)-1-piperazineethanesulfonic acid (HEPES) was purchased from VWR.

Synthesis of core-shell pNIPAM microgels

The microgels with fluorescent cores and thermo-responsive shells were prepared in a two-step synthesis [57]: first the PTFMA-cores containing a fluorescent dyes were prepared using free radical emulsion polymerization, then a shell of PNIPAM and PAA or PMAA co-polymer was grown by free radical precipitation polymerization around this core. For the cores, TFMA (10 mL; 12 g; 70,3 mmol), NIPAM (940 mg; 8,31 mmol), SDS (30 mg; 0,104 mmol) and Nile red (5 mg; 0.016 mmol) or BODIPY 493/503 (5 mg; 0,016 mmol) were added in water (30 mL) and stirred at 600 rpm for 20 min and purged with N₂. The reaction mixture was heated up to 70 °C. KPS (25 mg; 0.093 mmol), previously dissolved in water (2,5 mL), was added after the emulsion was stirred for 15 min at 70 °C. After 4 h of stirring at 70 °C the reaction was stopped by contact with air. The resulting particles were directly filtered. The purification of the particles was carried out via centrifugation followed by decantation, addition of Milli-Q water and particle redispersion. The purification via centrifugation was performed three times. To remove SDS residues, the redispersed particles were dialysed in water for 24 - 72 h (dialysis tube membrane: 12 - 14 kDa). The particles were analysed with dynamic light scattering (ZetaSizer Nano DLS).

The PNIPAM-co-AA / PNIPAM-co-MAA shells were grown by first dissolving NIPAM(1.15g), BIS(11.5 mg) and MAA or AA(88.5 µl) in 50 ml milli-Q water. Then 300 µl of the core particle suspension was added. The mixture was stirred at 600 rpm for 20 min and purged with N₂. The reaction mixture was heated up to 70 °C and KPS (25 mg; 0.093 mmol) was slowly added. After 2 h, the reaction reached completion and the microgel suspension was filtered and dialysed for 48h (dialysis tube membrane: 12 - 14 kDa). The particles were characterized with DLS.

Fabrication of colloidal molecules

The responsive microswimmers were prepared using sequential capillarity-assisted particles assembly (sCAPA). The basic principles of sCAPA are described by Ni et al.[19]. Here, we used an adapted version of sCAPA, which uses masters prepared with direct-writing via two-photon nanolithography, as opposed to Si masters made with conventional lithography methods. Briefly, negative masters were prepared with two-photon lithography (Nanoscribe Photonic Professional GT2) using an 63x oil-immersion objective and IP-Dip solution set.[34] The masters contained 6 smaller areas with 10,000 "traps" each, and one area was used to prepare the particles for one experiment. After printing and developing under standard conditions, these masters were post-cured for 2h under a UV-lamp and coated with a perfluorosilane using chemical vapor deposition. PDMS (Sylgard 184) was used to make templates from these masters. sCAPA was performed as described in the following paper [35]. The PS particles were deposited from a 0.035% Triton X-45 and 3.5 mM SDS solution in Milli-Q water. The microgels from a 0.04% Triton X-45 in 1 mM HEPES pH 7.4 or 0.025% Triton X-45 in 1 mM MES pH 4.5 for green and red-core microgels, respectively. All deposition were carried out at 25 ° C with a deposition rate of 3 µm s⁻¹.

Active motion experiments

The colloidal clusters were activated using AC electric fields in a closed cell with the top and bottom electrodes consisting of transparent conductive slides separated by a 240 µm-thick spacer (Grace Bio-Labs SecureSeal, USA, custom shape). The conductive slides were boro-silicate microscope slides coated with 3 nm Cr and 10 nm Au by thermal evaporation. The bottom slide on which the particles move was treated with thiolated polyethylene glycol (6 kDa, 1 mM in Milli-Q water, 30 min) to prevent sticking. The colloidal molecules were transferred from the sCAPA-templates to the top electrode, previously coated by a 3 µm-thick spin-coated layer of glucose (40% wt. in DI-water, 30 s 4000 rpm). Upon exposing the top slide to the suspending medium (0.1 mM HEPES buffer at pH 7 and 0.001% wt. Triton in Milli-Q water) and closing the cell, the glucose layer dissolved and the particles sedimented to the bottom electrode. The conductive slides were connected to function generator (Agilent 33500B) with copper leads made from 50 µm copper foil and the experiments were preformed on a Eclipse Nikon Ti2-e with a Lumencor Spectra II light box and a 20x objective. The particles were actuated by applying an AC field with 800 Hz frequency and 7 V peak-to-peak amplitude. The field was applied for 15 min to equilibrate the sample before collecting data. Movies were

recorded in a 1024*1024 px² window (340*340 μm²) at 10 frames per second. The local temperature was regulated through illumination with the 395 nm and 555 nm light sources of the light box (see SI for more details).

All the particles in the field of view were located and tracked using the TrackPy library in Python [58]. Stuck particles and particles that get stuck during the experiment were omitted from the analysis. The instantaneous velocity of every individual particle was determined by measuring their displacements over 0.5 s windows (5 frames). The angular velocity was determined by a least-square fit the auto-correlation function of the direction of motion over 30 s windows (see SI for more details), corresponding to the time windows over which temperature was changed.

References

- [1] Metin Sitti. Physical intelligence as a new paradigm. *Extreme Mechanics Letters*, 46:101340, 2021.
- [2] Ryan L. Truby. Designing Soft Robots as Robotic Materials. *Accounts of Materials Research*, 2(10):854–857, 2021.
- [3] Joyce C. Breger, Changkyu Yoon, Rui Xiao, Hye Rin Kwag, Martha O. Wang, John P. Fisher, Thao D. Nguyen, and David H. Gracias. Self-folding thermo-magnetically responsive soft microgrippers. *ACS Applied Materials and Interfaces*, 7(5):3398–3405, 2015.
- [4] Koohee Han, C. Wyatt Shields, Nidhi M. Diwakar, Bhuvnesh Bharti, Gabriel P. López, and Orlin D. Velev. Sequence-encoded colloidal origami and microbot assemblies from patchy magnetic cubes. *Science Advances*, 3(8):1–7, 2017.
- [5] Yong Dou and Kyle J. M. Bishop. Autonomous navigation of shape-shifting microswimmers. *Phys. Rev. Research*, 1:032030, Dec 2019.
- [6] Berta Esteban Fernández De Ávila, Pavimol Angsantikul, Jinxing Li, Miguel Angel Lopez-Ramirez, Doris E. Ramírez-Herrera, Soracha Thamphiwatana, Chuanrui Chen, Jorge Delezuk, Richard Samakapiruk, Valentin Ramez, Liangfang Zhang, and Joseph Wang. Micromotor-enabled active drug delivery for in vivo treatment of stomach infection. *Nature Communications*, 8(1):1–8, 2017.
- [7] Ana C. Hortelao, Cristina Simões, Maria Guix, Sandra Guallar-Garrido, Esther Julián, Diana Vilela, Luka Rejc, Pedro Ramos-Cabrer, Unai Cossío, Vanessa Gómez-Vallejo, Tania Patiño, Jordi Llop, and Samuel Sánchez. Swarming behavior and in vivo monitoring of enzymatic nanomotors within the bladder. *Science Robotics*, 6(52):eabd2823, 2021.
- [8] Mukrime Birgul Akolpoglu, Yunus Alapan, Nihal Olcay Dogan, Saadet Fatma Baltaci, Oncay Yasa, Gulsen Aybar Tural, and Metin Sitti. Magnetically steerable bacterial microrobots moving in 3d biological matrices for stimuli-responsive cargo delivery. *Sci. Adv*, 8:6163, 2022.
- [9] Varun Sridhar, Filip Podjaski, Yunus Alapan, Julia Kröger, Lars Grunenberg, Vimal Kishore, Bettina V Lotsch, and Metin Sitti. Light-driven carbon nitride microswimmers with propulsion in biological and ionic media and responsive on-demand drug delivery. *Sci. Robot*, 7:1421, 2022.
- [10] S. Schuerle, A. P. Soleimany, T. Yeh, G. M. Anand, M. Häberli, H. E. Fleming, N. Mirkhani, F. Qiu, S. Hauert, X. Wang, B. J. Nelson, and S. N. Bhatia. Synthetic and living micropropellers for convection-enhanced nanoparticle transport. *Science Advances*, 5, 2019.
- [11] Hong Wang, Bahareh Khezri, and Martin Pumera. Catalytic dna-functionalized self-propelled micromachines for environmental remediation. *Chem*, 1:473–481, 9 2016.
- [12] Ruiqin Wang, Weilin Guo, Xianghui Li, Zhonghua Liu, Hua Liu, and Shiyang Ding. Highly efficient mof-based self-propelled micromotors for water purification. *RSC Advances*, 7:42462–42467, 2017.
- [13] Songbo Ni, Emanuele Marini, Ivo Buttinoni, Heiko Wolf, and Lucio Isa. Hybrid colloidal microswimmers through sequential capillary assembly. *Soft Matter*, 13:4252–4259, 2017.
- [14] Zuochen Wang, Zhisheng Wang, Jiahui Li, Simon Tsz Hang Cheung, Changhao Tian, Shin Hyun Kim, Gi Ra Yi, Etienne Ducrot, and Yufeng Wang. Active patchy colloids with shape-tunable dynamics. *Journal of the American Chemical Society*, 141:14853–14863, 9 2019.
- [15] Rodrigo Soto and Ramin Golestanian. Self-assembly of catalytically active colloidal molecules: Tailoring activity through surface chemistry. *Physical Review Letters*, 112:068301, 2 2014.
- [16] Ran Niu, Thomas Palberg, and Thomas Speck. Self-assembly of colloidal molecules due to self-generated flow. *Physical Review Letters*, 119:028001, 7 2017.
- [17] Hartmut Löwen. Active colloidal molecules. *Europhysics Letters*, 121:58001, 4 2018.

- [18] L. Alvarez, M. A. Fernandez-Rodriguez, A. Alegria, S. Arrese-Igor, K. Zhao, M. Kröger, and Lucio Isa. Reconfigurable artificial microswimmers with internal feedback. *Nature Communications*, 12, 12 2021.
- [19] S. Ni, J. Leemann, I. Buttinoni, L. Isa, and H. Wolf. Programmable colloidal molecules from sequential capillarity-assisted particle assembly. *Science Advances*, 2:e1501779–e1501779, 2016.
- [20] W. D. Ristenpart, I. A. Aksay, and D. A. Saville. Electrohydrodynamic flow around a colloidal particle near an electrode with an oscillating potential. *Journal of Fluid Mechanics*, 575:83–109, 3 2007.
- [21] Fuduo Ma, Xingfu Yang, Hui Zhao, and Ning Wu. Inducing propulsion of colloidal dimers by breaking the symmetry in electrohydrodynamic flow. *Physical Review Letters*, 115, 11 2015.
- [22] Fuduo Ma, Sijia Wang, David T. Wu, and Ning Wu. Electric-field-induced assembly and propulsion of chiral colloidal clusters. *Proc. Natl. Acad. Sci. USA*, 112(20):6307–6312, 2015.
- [23] C. Wyatt Shields and Orlin D. Velev. The evolution of active particles: Toward externally powered self-propelling and self-reconfiguring particle systems. *Chem*, 3:539–559, 2017.
- [24] Wenjuan Su, Kongshuang Zhao, Jingjing Wei, and To Ngai. Dielectric relaxations of poly(n-isopropylacrylamide) microgels near the volume phase transition temperature: Impact of cross-linking density distribution on the volume phase transition. *Soft Matter*, 10:8711–8723, 11 2014.
- [25] P. S. Mohanty, S. Nöjd, M. J. Bergman, G. Nägele, S. Arrese-Igor, A. Alegria, R. Roa, P. Schurtenberger, and J. K.G. Dhont. Dielectric spectroscopy of ionic microgel suspensions. *Soft Matter*, 12:9705–9727, 2016.
- [26] A. Fernández-Nieves, A. Fernández-Barbero, B. Vincent, and F. J. De Las Nieves. Charge controlled swelling of microgel particles. *Macromolecules*, 33:2114–2118, 3 2000.
- [27] Andrea Ruscito, Ester Chiessi, Yosra Toumia, Letizia Oddo, Fabio Domenici, and Gaio Paradossi. Microgel particles with distinct morphologies and common chemical compositions: A unified description of the responsivity to temperature and osmotic stress. *Gels*, 6:1–19, 12 2020.
- [28] Christine Scherzinger, Annett Schwarz, André Bardow, Kai Leonhard, and Walter Richtering. Cononsolvency of poly-n-isopropyl acrylamide (pnipam): Microgels versus linear chains and macrogels. *Current Opinion in Colloid and Interface Science*, 19:84–94, 2014.
- [29] Chia Lung Lin, Wen Yen Chiu, and Chia Fen Lee. Preparation, morphology, and thermoresponsive properties of poly(n-isopropylacrylamide)-based copolymer microgels. *Journal of Polymer Science, Part A: Polymer Chemistry*, 44:356–370, 1 2006.
- [30] Karl Kratz, Thomas Hellweg, and Wolfgang Eimer. Influence of charge density on the swelling of colloidal poly(n-isopropylacrylamide-co-acrylic acid) microgels. *Colloids and Surfaces A: Physicochemical and Engineering Aspects*, 170, 2000.
- [31] Xiaoye Gao, Yue Cao, Xiangfu Song, Zhe Zhang, Chunsheng Xiao, Chaoliang He, and Xuesi Chen. Ph- and thermo-responsive poly(n-isopropylacrylamide-co-acrylic acid derivative) copolymers and hydrogels with lct dependent on ph and alkyl side groups. *Journal of Materials Chemistry B*, 1:5578–5587, 11 2013.
- [32] Jun Ho Son, Byungrae Cho, Soongweon Hong, Sang Hun Lee, Ori Hoxha, Amanda J. Haack, and Luke P. Lee. Ultrafast photonic pcr. *Light: Science and Applications*, 4, 7 2015.
- [33] COMSOL AB. Comsol multiphysics® v. 5.5., 2020.
- [34] Steven van Kesteren, Xueting Shen, Michele Aldeghi, and Lucio Isa. Printing on particles: combining two-photon nanolithography and capillary assembly to fabricate multi-material microstructures. *arXiv*, 10.48550/ARXIV.2208.02635, 2022.
- [35] Songbo Ni, Jessica Leemann, Heiko Wolf, and Lucio Isa. Insights into mechanisms of capillary assembly. *Faraday Discussions*, 181:225–242, 2015.
- [36] Howard Brenner. Coupling between the translational and rotational brownian motions of rigid particles of arbitrary shape ii. general theory. *JOURNAL OF COLLOID AND INTERFACE SCIENCE*, 23:407–436, 1967.
- [37] Ayan Chakrabarty, Andrew Konya, Feng Wang, Jonathan V. Selinger, Kai Sun, and Qi Huo Wei. Brownian motion of arbitrarily shaped particles in two dimensions. *Langmuir*, 30:13844–13853, 11 2014.
- [38] Zi Tong Zhang, Xin Zhao, and Bing Yang Cao. Diffusion tensors of arbitrary-shaped nanoparticles in fluid by molecular dynamics simulation. *Scientific Reports*, 9, 12 2019.
- [39] Daniela J. Kraft, Raphael Wittkowski, Borge Ten Hagen, Kazem V. Edmond, David J. Pine, and Hartmut Löwen. Brownian motion and the hydrodynamic friction tensor for colloidal particles of complex shape. *Physical Review E - Statistical, Nonlinear, and Soft Matter Physics*, 88, 11 2013.

- [40] R. J. Archer, A. I. Campbell, and S. J. Ebbens. Glancing angle metal evaporation synthesis of catalytic swimming janus colloids with well defined angular velocity. *Soft Matter*, 11:6872–6880, 7 2015.
- [41] Celia Lozano, Borge Ten Hagen, Hartmut Löwen, and Clemens Bechinger. Phototaxis of synthetic microswimmers in optical landscapes. *Nat. Commun.*, 7:12828, 2016.
- [42] Celia Lozano and Clemens Bechinger. Diffusing wave paradox of phototactic particles in traveling light pulses. *Nat. Commun.*, 10(1):2495, 2019.
- [43] Jochen Arlt, Vincent A. Martinez, Angela Dawson, Teuta Pilizota, and Wilson C.K. Poon. Painting with light-powered bacteria. *Nat. Commun.*, 9(1):768, 2018.
- [44] Giacomo Frangipane, Dario Dell’Arciprete, Serena Petracchini, Claudio Maggi, Filippo Saglimbeni, Silvio Bianchi, Gaszton Vizsnyiczai, Maria Lina Bernardini, and Roberto Di Leonardo. Dynamic density shaping of photokinetic *E. coli*. *eLife*, 7:1–14, 2018.
- [45] François A. Lavergne, Hugo Wendehenne, Tobias Bäuerle, and Clemens Bechinger. Group formation and cohesion of active particles with visual perception–dependent motility. *Science*, 364:70–74, 4 2019.
- [46] Utsab Khadka, Viktor Holubec, Haw Yang, and Frank Cichos. Active particles bound by information flows. *Nature Communications*, 9:3864, 2018.
- [47] Martin Fränzl and Frank Cichos. Active particle feedback control with a single-shot detection convolutional neural network. *Scientific Reports 2020 10:1*, 10:1–7, 7 2020.
- [48] Miguel Angel Fernandez-Rodriguez, Fabio Grillo, Laura Alvarez, Marco Rathlef, Ivo Buttinoni, Giovanni Volpe, and Lucio Isa. Feedback-controlled active brownian colloids with space-dependent rotational dynamics. *Nat. Commun.*, 11(1):4223, 2020.
- [49] Yuguang Yang and Michael A. Bevan. Optimal navigation of self-propelled colloids. *ACS Nano*, 12:10712–10724, 11 2018.
- [50] Mite Mijalkov, Austin McDaniel, Jan Wehr, and Giovanni Volpe. Engineering sensorial delay to control phototaxis and emergent collective behaviors. *Physical Review X*, 6:011008, 1 2016.
- [51] Mallika Das, Nicolas Sanson, Dnniele Fava, and Eugenia Kumacheva. Microgels loaded with gold nanorods: Photothermally triggered volume transitions under physiological conditions. *Langmuir*, 23:196–201, 2007.
- [52] Daisuke Suzuki and Ryo Yoshida. Temporal control of self-oscillation for microgels by cross-linking network structure temporal control of self-oscillation for microgels by cross-linking network structure. *Science And Technology*, pages 5830–5838, 2008.
- [53] Supparesk Rittikulsittichai, Arati G. Kolhatkar, Subhasis Sarangi, Maria A. Vorontsova, Peter G. Vekilov, Audrius Brazdeikis, and T. Randall Lee. Multi-responsive hybrid particles: Thermo-, ph-, photo-, and magneto-responsive magnetic hydrogel cores with gold nanorod optical triggers. *Nanoscale*, 8:11851–11861, 2016.
- [54] Zhuo Tang, Ying Guan, and Yongjun Zhang. Contraction-type glucose-sensitive microgel functionalized with a 2-substituted phenylboronic acid ligand. *Polymer Chemistry*, 5:1782–1790, 3 2014.
- [55] Marc Hippler, Eva Blasco, Jingyuan Qu, Motomu Tanaka, Christopher Barner-Kowollik, Martin Wegener, and Martin Bastmeyer. Controlling the shape of 3d microstructures by temperature and light. *Nature Communications*, 10, 12 2019.
- [56] Xinghao Hu, Immihan C. Yasa, Ziyu Ren, Sandhya R. Goudu, Hakan Ceylan, Wenqi Hu, and Metin Sitti. Magnetic soft micromachines made of linked microactuator networks. *Science Advances*, 7, 6 2021.
- [57] Dennis Go, Thomas E. Kodger, Joris Sprakel, and Alexander J.C. Kuehne. Programmable co-assembly of oppositely charged microgels. *Soft Matter*, 10:8060–8065, 10 2014.
- [58] Daniel B. Allan, Thomas Caswell, Nathan C. Keim, Casper M. van der Wel, and Ruben W. Verweij. soft-matter/trackpy: Trackpy v0.5.0, 2021.